Novel Murine Model of Chronic Granulomatous Lung Inflammation Elicited by Carbon Nanotubes

Isham Huizar[1], Anagha Malur[1], Yasmeen A. Midgette[1], Cindy Kukoly[1], Pengyu Chen[4], Pu Chun Ke[5], Ramakrishna Podila[5], Apparao M. Rao[5], Christopher J. Wingard[2], Larry Dobbs[3], Barbara P. Barna[1], Mani S. Kavuru[1], and Mary Jane Thomassen[1]

[1]Division of Pulmonary, Critical Care, and Sleep Medicine, Department of Internal Medicine, [2]Department of Physiology, and [3]Department of Pathology, Brody School of Medicine, East Carolina University, Greenville, North Carolina; and [4]Department of Electrical and Computer Engineering, and [5]Department of Physics and Astronomy, Clemson University, Clemson, South Carolina

Lung granulomas are associated with numerous conditions, including inflammatory disorders, exposure to environmental pollutants, and infection. Osteopontin is a chemotactic cytokine produced by macrophages, and is implicated in extracellular matrix remodeling. Furthermore, osteopontin is up-regulated in granulomatous disease, and osteopontin null mice exhibit reduced granuloma formation. Animal models currently used to investigate chronic lung granulomatous inflammation bear a pathological resemblance, but lack the chronic nature of human granulomatous disease. Carbon nanoparticles are generated as byproducts of combustion. Interestingly, experimental exposures to carbon nanoparticles induce pulmonary granuloma-like lesions. However, the recruited cellular populations and extracellular matrix gene expression profiles within these lesions have not been explored. Because of the rapid resolution of granulomas in current animal models, the mechanisms responsible for persistence have been elusive. To overcome the limitations of previous models, we investigated whether a model using multiwall carbon nanoparticles would resemble chronic human lung granulomatous inflammation. We hypothesized that pulmonary exposure to multiwall carbon nanoparticles would induce granulomas, elicit a macrophage and T-cell response, and mimic other granulomatous disorders with an up-regulation of osteopontin. This model demonstrates: (*1*) granulomatous inflammation, with macrophage and T-cell infiltration; (*2*) resemblance to the chronicity of human granulomas, with persistence up to 90 days; and (*3*) a marked elevation of osteopontin, metalloproteinases, and cell adhesion molecules in granulomatous foci isolated by laser-capture microdissection and in alveolar macrophages from bronchoalveolar lavage. The establishment of such a model provides an important platform for mechanistic studies on the persistence of granuloma.

Keywords: granuloma; carbon nanotube; murine model; osteopontin; matrix metalloproteinases

Granuloma formation is thought to play a critical role in the elimination of bacteria, fungi, and parasites. Granulomatous inflammation also occurs as a response to an "innocuous" foreign body, and in some conditions (e.g., sarcoidosis, granulomatosis with polyangiitis [Wegener's], and rheumatoid arthritis), the etiologic agent has not been established (1–7). To study granulomatous disorders, various animal models were developed, and significant findings related to granulomatous inflammation were elucidated from these models. A major advance occurred with the development of a murine granuloma model in which antigen-bound sepharose beads were injected intravenously into presensitized animals (8). Although this model contributed to our current understanding, the resolution of granulomas within 14–21 days comprises its major disadvantage. Because of the rapid disappearance of granulomas, various changes in gene and protein (e.g., cytokines, proteases, and transcription factors) expression may reflect either the initial or resolution phase of the inflammatory response, rather than factors contributing to the persistence of granulomatous inflammation. Another consideration involves the delivery route, namely, a tail-vein injection of antigen-bound sepharose beads that lodges in the pulmonary circulation rather than directly in the alveolar space (8, 9).

Studies of experimental animal models noted acute inflammation and/or pulmonary granuloma-like lesions in association with aggregated carbon nanoparticles (10–12). Carbon nanoparticles were found as byproducts of combustion (e.g., diesel, methane, propane, and natural-gas flames of typical stoves) (10, 11). In fact, a sarcoid-like disease in firefighters and others was described after exposure to combustion byproducts, and carbon nanoparticles were found postmortem in lung tissue (13–16). Carbon-based nanomaterials have emerged as a new technology with unique applications in multiple industries, and the use of nanomaterials in consumer products is a rapidly expanding area of manufacturing. Already, numerous products containing nanomaterials are on the market, from sunscreens to bicycle frames. Because of their unique physiochemical characteristics, nanomaterials may exert unique toxicological effects which have not been fully investigated.

Regardless of the cause of granulomatous inflammation, a model that resembles such a process will aid in understanding the mechanisms of granulomatous inflammation, and will provide therapeutic targets for disease modification. Osteopontin is a key cytokine recently shown to associate with granulomatous inflammation, regardless of cause (17–20). Osteopontin induces leukocyte chemotaxis, and is produced by alveolar macrophages. Interestingly, osteopontin null mice exhibit reduced formation of granulomas in response to infectious stimuli (21). Based on these observations, we hypothesized that pulmonary exposure to multiwall carbon nanoparticles (MWCNTs) would induce granulomas, elicit a macrophage and T-cell response, and mimic other granulomatous disorders with the up-regulation of osteopontin. Furthermore, such changes would present an appearance clearly distinct from that of adjacent, normal lung tissue, with altered bronchoalveolar lavage (BAL) cell gene expression, but not as pronounced as within granulomatous foci. To address this hypothesis, we instilled mice with MWCNTs and evaluated lung changes up to 90 days after exposure. Granulomatous foci were dissected by laser-capture microdissection (LCM), and BAL cells were analyzed for cellular and gene expression changes.

(*Received in original form September 28, 2010 and in final form February 3, 2011*)

This work was supported by North Carolina Biotechnology Center grant BRG-1206.

Correspondence and requests for reprints should be addressed to Isham Huizar, M.D., Division of Pulmonary, Critical Care, and Sleep Medicine, Department of Internal Medicine, Brody School of Medicine, East Carolina University, 3E-149 Brody Medical Sciences Building, Greenville, NC 27834. E-mail: huizari@ecu.edu

This article has an online supplement, which is accessible from this issue's table of contents at www.atsjournals.org

Am J Respir Cell Mol Biol Vol 45. pp 858–866, 2011
Originally Published in Press as DOI: 10.1165/rcmb.2010-0401OC on March 18, 2011
Internet address: www.atsjournals.org

MATERIALS AND METHODS

Animals

C57Bl/6 mice were purchased from Jackson Laboratory (Bar Harbor, ME). This study was approved by the East Carolina University Institutional Animal Care Committee (AUP#J199).

Characterization of Carbon Nanotubes

MWCNTs (catalogue number 900–1501, lot GS1801), grown via chemical vapor deposition, were obtained from SES Research (Houston, TX). We determined the structure of MWCNTs by scanning electron microscopy. Nitrogen adsorption studies were performed using a physisorption analyzer (ASAP 2010; Micromeritics, Norcross, GA). Catalyst content was measured using a Thermogravimetric Analyzer Pyris 1 TGA (Perkin-Elmer, Waltham, MA). MWCNT samples were placed in a platinum pan ($\sim$ 0.1–0.2 cm^3) to fill 40–50% of the pan volume, and were heated from 30°C to 800°C at a rate of 20°C/minute in an air atmosphere (using an airflow rate of 20 ml/min). Dynamic light-scattering (DLS) was performed using a Nanosizer S90 (Malvern Instruments, Worcestershire, UK), and the zeta potential of MWCNT suspension was determined using a Zeta ZS (Malvern Instruments). MWCNTs were dispersed in a saline solution containing 35% surfactant (Infrasurf; a gift of ONY, Inc., Amherst, NY) at 2 μg/μl, and the mixture was bath-sonicated (model 1510R-MTH; Branson Ultrasonics Corp. Danbury, CT) for 45 minutes to obtain a suspension.

Instillation of Carbon Nanotubes

An oropharyngeal instillation was performed after sedation with isofluorane. Gently pulling forward the mouse tongue exposed the epiglottis, and a 50-μl volume was instilled using a pipette. Procedures were performed according to the East Carolina University Office of Environmental Health and Safety within an approved fume hood, to minimize exposure to the outside environment. Animals received 35% surfactant/saline (sham) or a 35% surfactant/saline solution containing 100 μg of MWCNT. On Days 10, 60, or 90 after exposure, the mice were killed, and BAL or lungs were harvested for further analysis.

Bronchoalveolar Lavage

BAL cells were obtained as previously described (22).

Histological Analysis

Lungs were dissected and fixed in PBS-buffered 4% formaldehyde. Lung sections stained with hematoxylin and eosin were evaluated by an experienced pathologist. Tissue slides were captured using ImageScope software, version 10.2.1.2314 (Aperio Technologies, Vista, CA). MWCNTs were located using histogram analysis of the captured tissue slide image, and were counted using ImageScope software.

Immunohistochemistry

Lungs were dissected, embedded in OCT (Tissue-Tek; Sakura Finetek, Torrance, CA), and frozen. Tissue sections or BAL cytospin slides were fixed with 4% paraformaldehyde–PBS, permeabilized with Triton X-100, and stained with antibodies to osteopontin (1:100), monocyte + macrophage-2 (1:25), CD3 (1:50), CD4 (1:50), or CD8 (1:50; ABCAM, Cambridge, MA), followed by Alexa-conjugated goat anti-rabbit IgG or goat anti-rat IgG (Invitrogen, Carlsbad, CA). Slides were counterstained with 4′,6-diamidino-2-phenylindole (Invitrogen) or propidium iodide (Vector Laboratories, Burlingame, CA) to facilitate nuclear localization.

Laser-Capture Microdissection

Granulomatous, nongranulomatous (normal-appearing lung tissue, away from the granulomas of mice exposed to MWCNTs), and normal tissue (sham-treated) was dissected using a Zeiss PALM IV LCM (Carl Zeiss MicroImaging LLC, Thornwood, New York) system from frozen sections of the lung. Tissue sections (7 μm) were mounted on membrane slides and processed using a modified protocol for LCM, as recommended by the handbook from Zeiss Microimaging GmbH. Tissue sections underwent dehydration and fixation in 70% and 100% ethanol for 3 minutes, followed by an additional washing in diethylpyrocarbonate–treated water to remove excess OCT. Sections were then stained in 1% cresyl violet, followed by washes in 70% and 100% ethanol (all solutions were ice-cold). Finally, slides were allowed to air-dry. Excised tissues

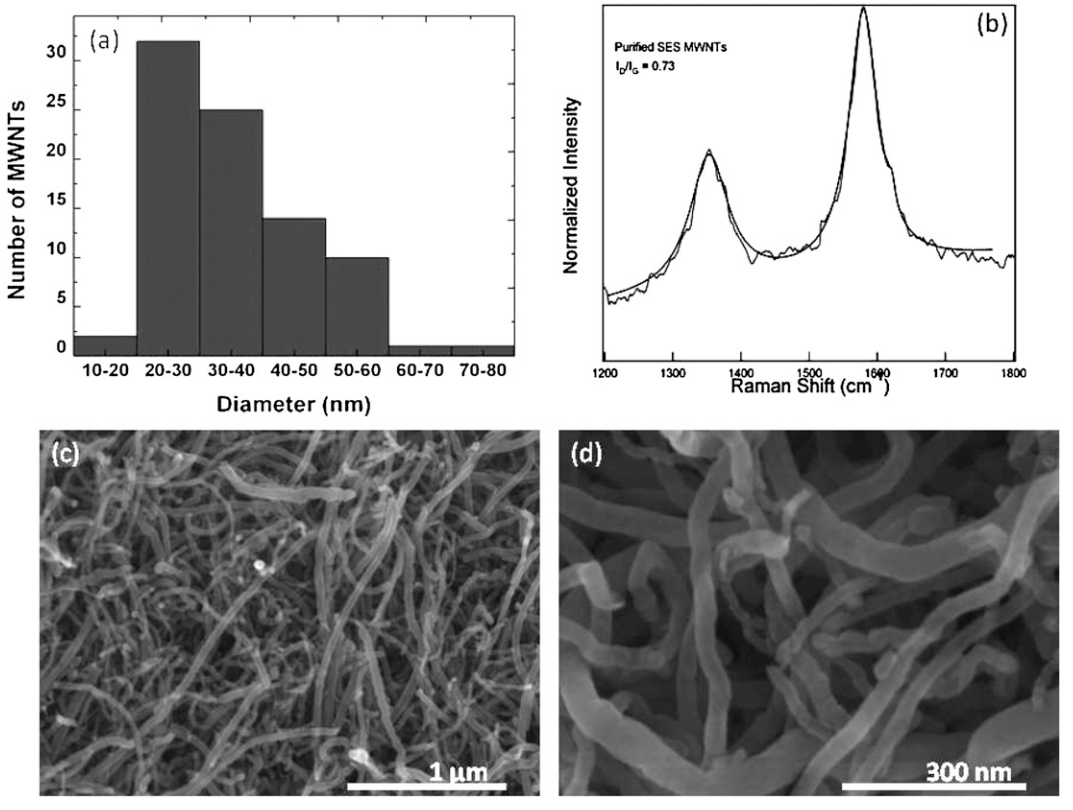

Figure 1. (*a*) Diameter distribution of multiwall carbon nanotubes (MWCNTs) obtained from scanning electron microscopy images in *c* and *d*. (*b*) Raman spectrum of MWNTs reveals presence of a D peak ($\sim$1,350 cm^{-1}), G peak ($\sim$1,580 cm^{-1}), and D′ peak (1,620 cm^{-1}). (*c* and *d*) Typical scanning electron microscopy images of MWCNTs.

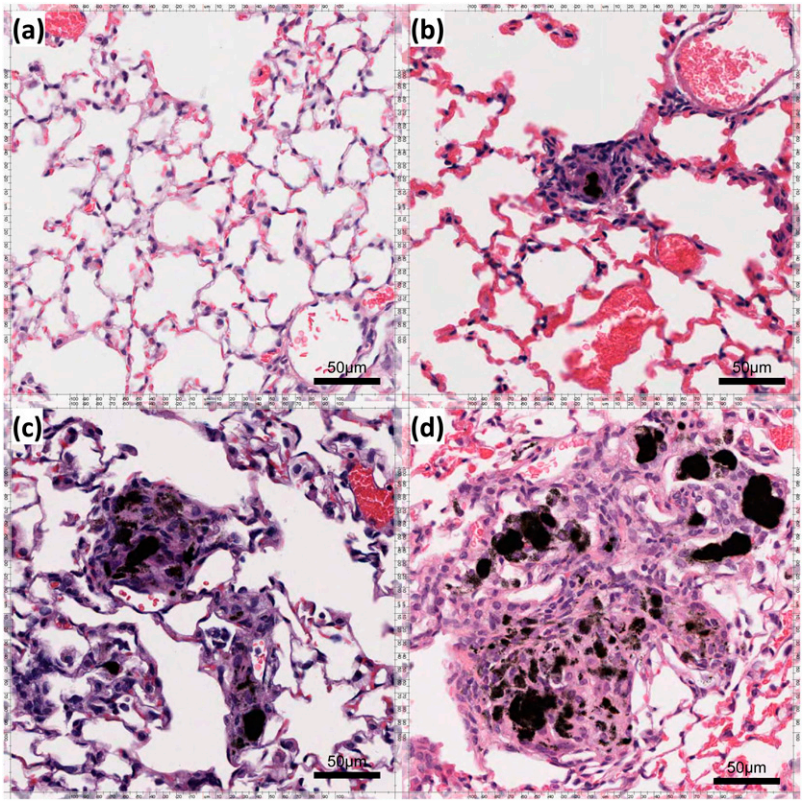

Figure 2. Persistence of granulomatous inflammation for up to 90 days after exposure to MWCNTs. Hematoxylin and eosin staining was applied to (*a*) murine lung control tissue and to murine lung tissue (*b*) 10 days, (*c*) 60 days, and (*d*) 90 days after exposure to MWCNTs. The granulomatous reaction surrounding MWCNT aggregates begins 10 days after exposure, and persists for 60 and 90 days after exposure to MWCNTs, without apparent resolution.

were collected into RLT buffer (Qiagen, Valencia, CA). RNA was extracted, converted into cDNA, or preamplified, as described later.

RNA Purification, Arrays, and Real-Time PCR

Total RNA was extracted from frozen lung tissue collected at the previously mentioned time points, using the RNeasy kit and protocol (Qiagen). Real-time PCR of total RNA from BAL cells was performed using an ABI Prism 7300 system (Applied Biosystems. Culver City, CA). Predesigned primers and probes for osteopontin, matrix metalloproteinases (MMPs), and glyceraldehyde 3–phosphate dehydrogenase as endogenous control were obtained from ABI. LCM samples (40 ng total RNA) underwent a preamplification step, using an RT^2 NanoPreAMP cDNA Synthesis Kit and Primer Mixes (SABiosciences, Frederick, MD). The quantification of gene expression for MMPs, tissue inhibitors of MMPs (TIMPs), and adhesion molecules was performed using the RT^2 Profiler PCR Array PAMM-013 (SABiosciences). Cytokines were measured with an RT^2 Profiler PCR Array PAMM 011 (SABiosciences) and the HT7900 Fast Real-Time PCR System (ABI). Product amplification was measured and analyzed as previously described, according to the manufacturer's instructions (22, 23).

Analysis of Osteopontin Protein

Murine osteopontin was quantified according to an ELISA assay (catalogue number DY441; R&D Systems, Minneapolis, MN).

Statistical Analysis

Data were analyzed by one-way ANOVA and the Student *t* test, using Prism software (GraphPad, Inc., La Jolla, CA) and MS Excel (Microsoft, Seattle, WA). Significance was defined as $P < 0.05$. Results are expressed as mean ± SEM.

RESULTS

Characterization of Carbon Nanotubes

Scanning electron microscopy revealed a dominant distribution of tube diameters in the range of 20–40 nm (Figure 1a). MWCNTs appeared to contain structural wall defects that were quantified by the Raman spectrum shown in Figure 1b. Strong disorder-induced Raman peaks were present at approximately 1,350 cm^{-1} and approximately 1,620 cm^{-1}, corresponding to the so-called D and D′ peaks, respectively. The ratios of D and D′ peaks relative to the graphite (G peak) were 0.73 and 0.22, respectively, indicating the presence of internal disorder in these samples. Figures 1c and 1d provide lower-magnification scanning electron microscopy images of MWCNTs. The surface area of MWCNTs was calculated as 85.75 m^2/g, according to the BET theory and nitrogen adsorption studies (24). Pore volume and pore-size distribution were measured according to the Barrett–Joyner–Halenda method (25). The pore volume (defined as the sum of volumes of all pores in 1 g of adsorbent) was 0.22 cm^3/g. To determine the purity of MWCNTs, catalyst content was measured with thermogravimetric analysis. We found that the net metal catalyst (Fe) content in MWCNTs was below 1 weight percent. The stability of the suspension was also evaluated by examining absorbance over time. We found a 21% reduction in absorbance measured at 320 nm over 24 hours for our MWCNT suspension, and no visible precipitation of the MWCNTs was evident when the suspension was stored overnight (data not shown). Combined with DLS (Figure E1 in the online supplement), measurements of zeta potential (Figure E2) suggest that this suspension of MWCNTs was stable and did not readily develop larger aggregates that would precipitate easily. Further detailed characteristics of the MWCNTs are described in the online supplement, and Figure E3 presents a typical optical microscope image of an MWCNT suspension.

Persistence of Granulomatous Inflammation up to 90 Days after Exposure to MWCNTs

Mice were instilled with escalating doses of MWCNTs (25, 50, and 100 μg). Doses of 25 and 50 μg resulted in minimal granulomatous responses (data not shown). A dose of 100 μg

TABLE 1. TOTAL NUMBERS AND DIFFERENTIAL COUNTS OF CELLS FROM BRONCHOALVEOLAR LAVAGE OF SHAM-TREATED CONTROL MICE, AND AFTER 60 AND 90 DAYS IN MICE INSTILLED WITH NANOTUBES

	Control Mice ($n = 14$)				60 Days ($n = 16$)				90 Days ($n = 16$)			
	AMs (%)	L (%)	PMN (%)	Total Cells (x 10^5)	AMs (%)	L (%)	PMN (%)	Total Cells (x 10^5)	AMs (%)	L (%)	PMN (%)	Total Cells (x 10^5)
Mean	99.3	0.6	0.1	5.5	99.1	0.8	0.1	4.9	99.9	0	0.1	4.3
± SEM	0.1	0.1	0	0.1	0.1	0.1	0	0.2	0	0	0	0.2

Definition of abbreviations: AMs, alveolar macrophages; L, lymphocytes; PMN, polymorphonuclear.

MWCNT was found to produce a marked granulomatous inflammatory response. Therefore, all subsequent experiments were performed with 100 μg of MWCNT. Compared with control samples (Figure 2a), the lungs of animals exposed to MWCNTs developed granulomatous lesions, first evident at 10 days after the instillation of MWCNTs (Figure 2b), although the granulomas identified were relatively small and poorly formed. At 60 days, well-formed granulomas containing MWCNT aggregates were easily found (Figure 2c). The granulomas showed macrophage infiltrates, and many of the macrophages comprising the granulomas had taken on a spindle shape, with a "swirling" pattern of growth that is characteristic of well-formed granulomas. These well-formed granulomas and associated MWCNTs persisted, and were still present at 90 days after exposure

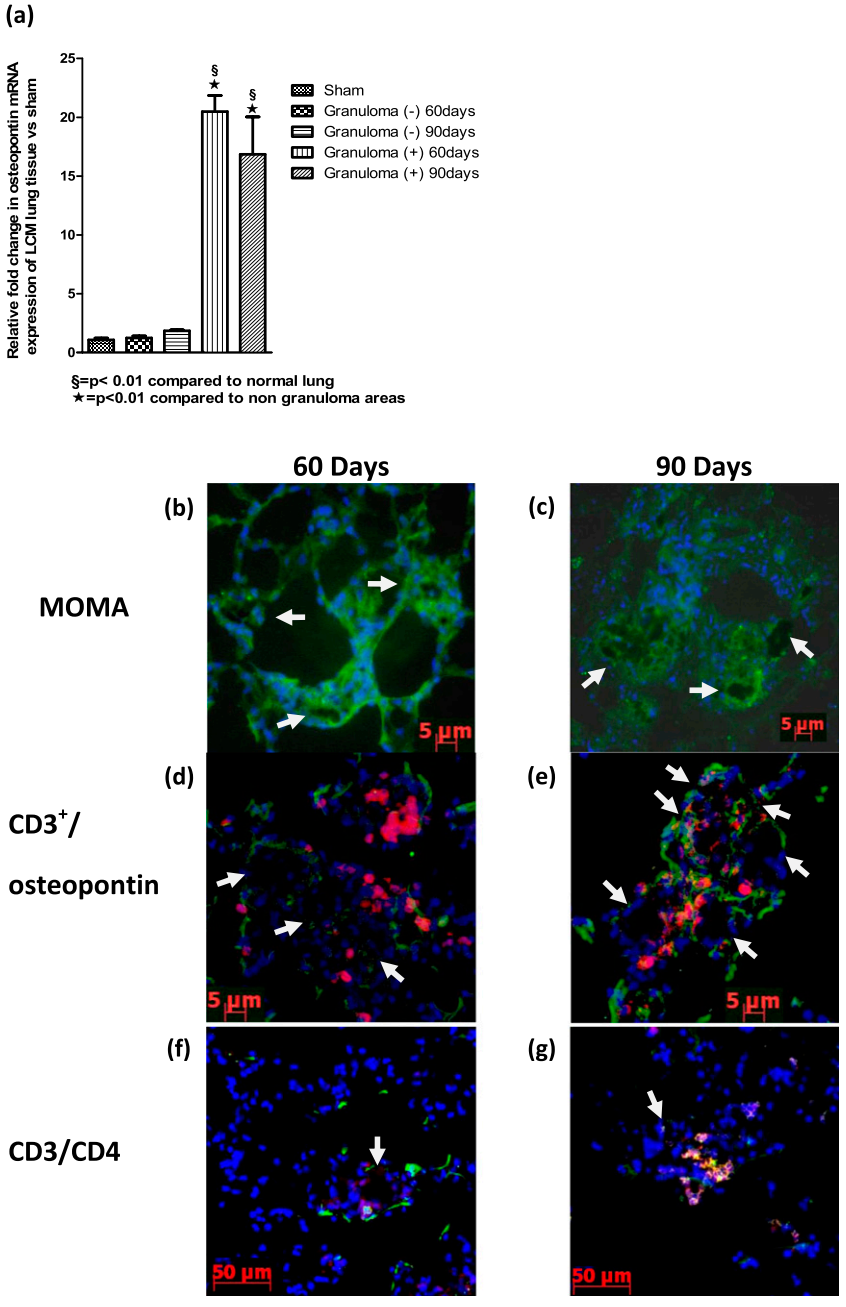

Figure 3. The expression of osteopontin mRNA is upregulated in granulomatous foci. (*a*) Osteopontin gene expression of lung tissue obtained through laser-capture microdissection (LCM) in sham untreated mice, surrounding normal lung tissue [Granuloma (−)] and granulomatous foci [Granuloma (+)]. The recruitment of $CD3^+$ T cells and macrophages, with fusion and multinucleated giant cells, is evident. Immunohistochemistry for macrophages (monocyte + macrophage [MOMA]; *green*) demonstrates macrophages surrounding MWCNT aggregates, (*b*) 60 days and (*c*) 90 days after exposure to MWCNTs. (*d* and *e*) Immunohistochemistry for $CD3^+$ T cells (*red*) and osteopontin (*green*) found within granulomatous lesions of murine lungs, (*d*) 60 days and (*e*) 90 days after exposure to MWCNTs. (*f* and *g*) Immunohistochemistry for $CD3^+$ T cells (*red*) and $CD4^+$ (*green*) in murine lungs, (*f*) 60 days and (*g*) 90 days after exposure to MWCNTs. *Arrows* indicate locations of MWCNT aggregates.

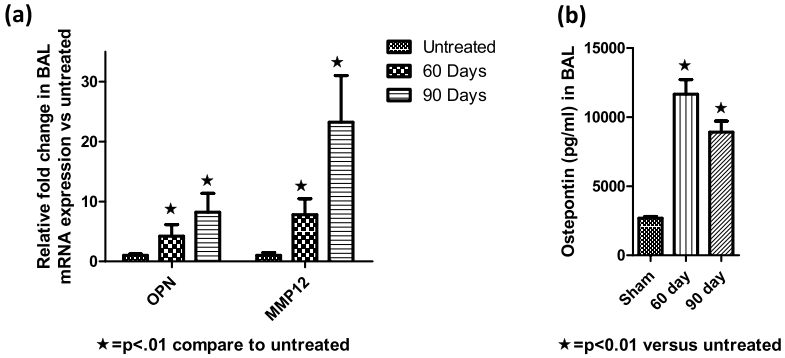

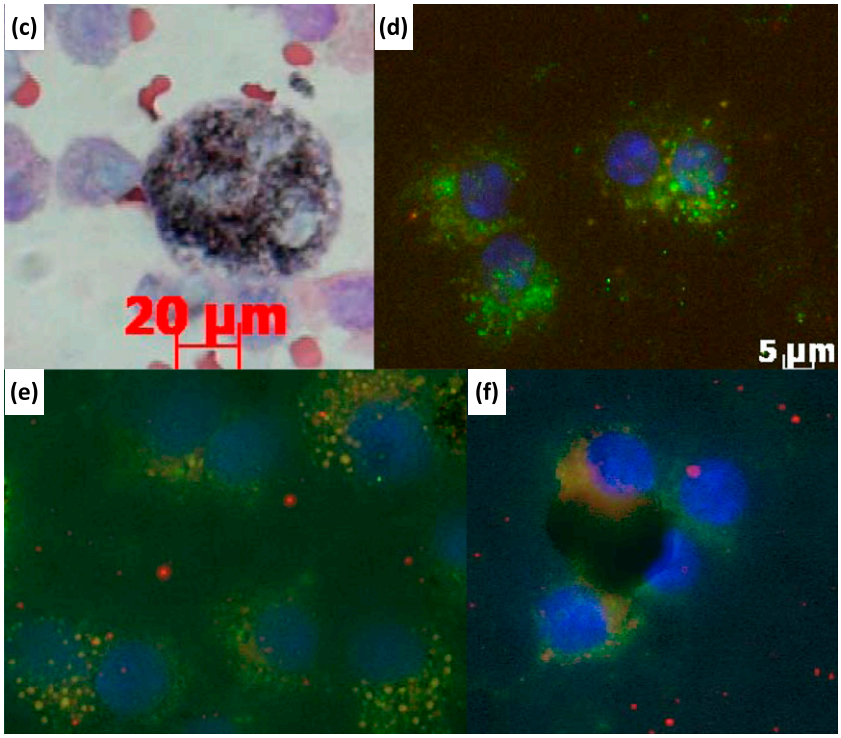

Figure 4. Osteopontin is increased in bronchoalveolar lavage (BAL) from mice exposed to MWCNTs at 60 and 90 days. (*a*) mRNA gene expression for matrix metalloproteinases (MMPs) in BAL, 60 and 90 days after exposure to MWCNTs. (*b*) Osteopontin protein concentrations in BAL, 60 and 90 days after exposure to MWCNTs. (*c*) Cytospin of BAL 90 days after exposure to MWCNTs reveals a macrophage-containing MWCNT within the cytoplasm. (*d–f*) Immunohistochemistry stain of BAL for macrophage marker MOMA (*green*), osteopontin (*red*), and overlap (*orange*) in (*d*) control mice, and (*e*) 60 days and (*f*) 90 days after exposure to MWCNTs.

(Figure 2d). Histological analysis of lung sections revealed MWCNTs spread across all lobes of the lung (Figure E4 depicts a representative section of lung tissue, 60 days after exposure to MWCNTs). The average MWCNT aggregates detected in tissue sections at 60 days comprised 720 ± 100 ($n = 4$) and 653 ($n = 6$) at 90 days. We did not find a significant deposition of collagen around the granulomas (Figure E5). To determine if the alveolar cell population had changed, specifically with respect to increased lymphocytes or neutrophils, BAL was collected at 60 and 90 days after exposure to MWCNTs. Total and differential cell counts were evaluated and compared with sham controls. All BAL samples contained more than 98% macrophages, with no significant change in cell numbers or differentials at 60 and 90 days compared with sham control samples (Table 1). The mean viability of lavage cells was greater than 95%, as determined by trypan blue dye exclusion.

Expression of Osteopontin mRNA Is Up-Regulated in Granulomatous Foci

Previous studies suggest osteopontin is a critical player in the formation of granulomas (18, 26). Therefore, we investigated osteopontin in MWCNT-induced granulomas. We compared granulomatous foci with nongranulomatous lung tissue isolated by LCM. Total RNA was then extracted and analyzed for osteopontin gene expression. Osteopontin was significantly ($P < 0.01$) up-regulated, with a 20-fold increase at 60 days

TABLE 2. MRNA FOLD CHANGE OF SELECTED CYTOKINES FROM LUNG GRANULOMA TISSUE OBTAINED WITH LCM, COMPARED WITH LUNG TISSUE OF CONTROL MICE

Cytokine Profile of mRNA Fold Change in LCM Granulomas			
Th1	Gene	60 Days	90 Days
	TNFRSF1b	3*	2
	TNF-α	2	8*
	IL-18	2*	5*
Th2	CCL7 (MCP-3)	7*	6*
	CCL11 (eotaxin)	7*	Unchanged
	IL-10	5	10*
Other chemokines	CCL2 (MCP-1)	6*	16*
	CCL22 (SCYA2)	6*	5*
	CCL20 (MIP-3α)	27*	92*
	CCL9 (MIP-1γ)	3*	8*

Definition of abbreviations: CCL, chemokine (C-C motif) ligand; LCM, laser-capture microdissection; MCP, monocyte chemotactic protein; MIP, macrophage inflammatory protein; SYCA2, small inducible cytokine A2; TNFRSF1b, tumor necrosis factor receptor superfamily member 1B.

* $P < 0.05$.

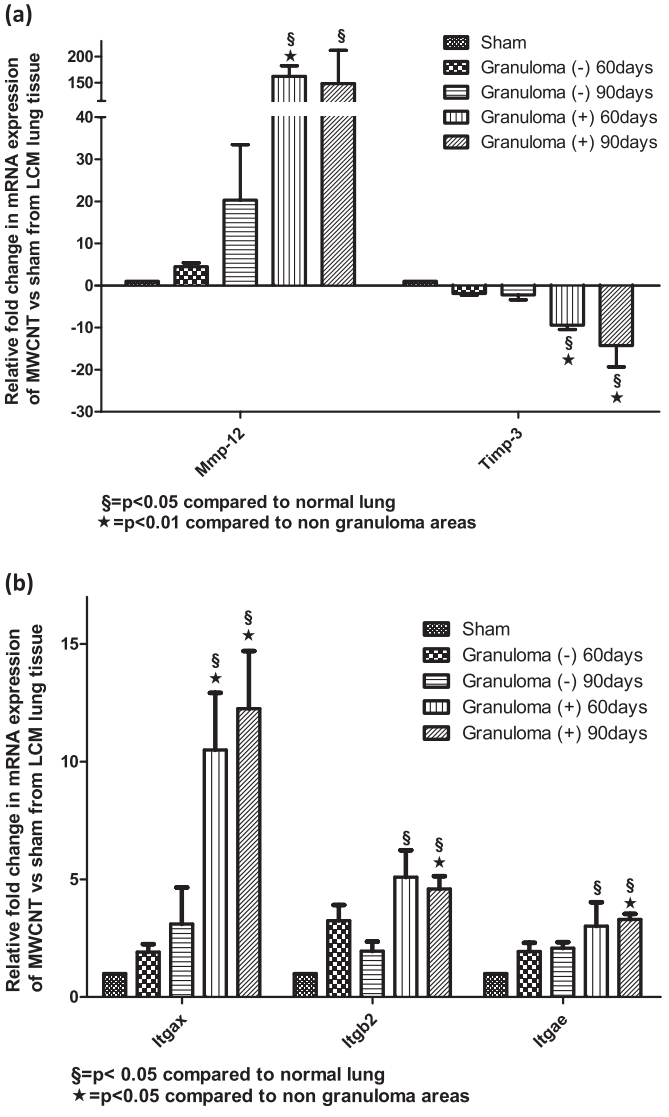

Figure 5. (*a*) Granulomatous foci are associated with an up-regulation in matrix proteases and a down-regulation of tissue inhibitor of metalloproteinases (TIMP)–3. The mRNA gene expression of MMPs and TIMP-3 was obtained from a PCR gene array of lung tissue via LCM from sham untreated mice, unaffected lung tissue [Granuloma (−)], and granulomatous foci [Granuloma (+)]. (*b*) Integrins (Itgs) are elevated within granulomatous foci at 60 and 90 days after exposure to MWCNTs. The mRNA gene expression of integrins was obtained from a PCR gene array of lung tissue obtained via LCM from sham untreated mice, unaffected lung [Granuloma (−)], and granulomatous foci [Granuloma (+)]. Itgs are elevated within granulomatous foci at 60 and 90 days after exposure to MWCNTs.

and a 17-fold increase at 90 days, whereas nongranulomatous tissue did not differ from untreated lung tissue (Figure 3a).

Recruitment of CD3$^+$ T Cells and Macrophages

T cells and macrophages were associated with granulomatous lesions (1, 27, 28). To characterize MWCNT-induced granulomas further, immunohistochemistry for macrophages (MOMA), T cells (CD3$^+$), and osteopontin was performed (Figure 3). Macrophages were localized within MWCNT-induced granulomas at both 60 and 90 days (Figures 3b and 3c). CD3$^+$ T cells were also evident within MWCNT-induced granulomas at 60 and 90 days (Figures 3d and 3e). Earlier time points did not reveal a significant granulomatous reaction (data not shown). Osteopontin was expressed in granulomas in close proximity to CD3$^+$ T cells (Figures 3c and 3d). Further analysis of CD3$^+$ lymphocytes revealed predominantly CD4$^+$ T cells (Figures 3e and 3f) and infrequent CD8$^+$ T cells (data not shown). To assist in the visualization of MWCNTs within granulomas on immunohistochemistry, inverted images of MWCNTs were included in the online supplement (Figure E6).

Osteopontin Is Increased in BAL from Mice Exposed to MWCNTs at 60 and 90 Days

To investigate whether osteopontin was elevated in the alveolar spaces, BAL was collected. BAL cells obtained 60 and 90 days after exposure to MWCNTs showed an up-regulated mRNA expression of osteopontin (fourfold at 60 days, and eightfold at 90 days). Osteopontin was shown to up-regulate matrix metalloproteinases (MMPs), and is elevated in granulomatous disorders (17). Therefore, we analyzed the expression of MMPs in BAL cells. MMP-12 was elevated eightfold at 60 days, and 23-fold at 90 days (Figure 4a). The concentration of osteopontin protein was significantly elevated in BAL fluid, 60 (11,650 pg/ml) and 90 (8,912 pg/ml) days after exposure to MWCNTs (Figure 4b). Macrophages obtained by BAL at 60 and 90 days after exposure contained MWCNTs (Figure 4c). Compared with control samples (Figure 4d), the immunohistochemistry of BAL cells revealed increased osteopontin protein expression in alveolar macrophages at 60 and 90 days (Figures 4e and 4f).

T-Cell and Cytokine Profiles of Lung-Tissue Granulomas

As already noted, differential analyses of BAL cells from mice exposed to MWCNTs did not indicate increases in lymphocytes, suggesting a lack of pulmonary directed T-cell response. However, CD3$^+$ T cells were present in granulomatous foci (Figures 3b–3g). To analyze the potential contributions of T cells further, we profiled inflammatory cytokines from LCM-isolated granulomas with a targeted PCR array (Table 2). Results indicated an elevation (> 2-fold) of cytokines associated with Th1 and Th2 cells, suggesting a mixed T-cell response. Cytokines associated with Th17 cells had not changed. Among the elevated Th1-associated cytokines were IL-1α, tumor necrosis factor receptor superfamily member 1B, TNF-α, and IL-18. Elevated Th2-associated cytokines included chemokine (C-C motif) ligand (CCL)-7 (monocyte chemotactic protein [MCP]-3), CCL11 (eotaxin), IL-10, and IL-13. The chemokines CCL2 (MCP-1), CCL22 (small inducible cytokine A2), CCL10 (macrophage inflammatory protein [MIP]-3α), and CCL9 (MIP-1γ), known to be associated with the recruitment of macrophages, were significantly ($P < 0.05$) elevated in LCM granulomas at 60 and 90 days after exposure to MWCNTs.

Granulomatous Foci Are Associated with Up-Regulation of MMP-12 and Down-Regulation of TIMP-3

For LCM samples, we used an RT-PCR gene array to scrutinize extracellular matrix changes in granulomatous foci, nongranulomatous tissue, and control tissue from untreated mice (see Materials and Methods). Granulomatous foci contained significantly ($P < 0.05$) elevated MMP-12, with a 162-fold increase at 60 days and a 148-fold increase at 90 days (Figure 5a). Concomitantly, a down-regulation of TIMP-3 occurred, with a 9.4-fold decrease at 60 days, and a 14.3-fold decrease at 90 days ($P < 0.05$) (Figure 5a).

Integrins Are Elevated within Granulomatous Foci at 60 and 90 Days after Exposure to MWCNTs

The fusion of macrophages into multinucleated giant cells involves adhesion molecules such as integrins α, β1, and β2

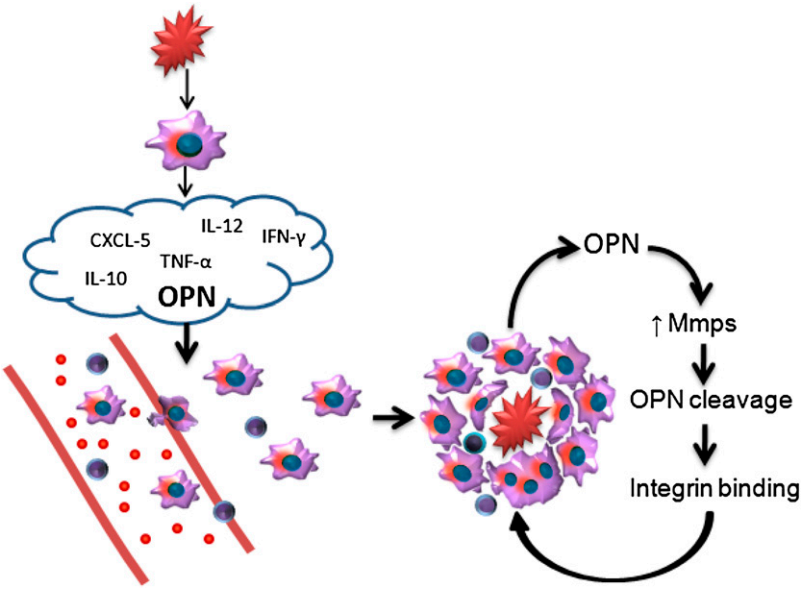

Figure 6. Proposed mechanisms for the formation of granulomas. The initial insult causes a release of cytokines, with subsequent recruitment, attachment, and transformation of macrophages and T cells. Osteopontin (OPN) within granulomas is proteolytically cleaved by MMPs binding to integrins and enabling macrophage fusion. These events result in the continued expression of osteopontin and MMPs, with subsequent transformation of macrophages into epithelioid and multinucleated giant cells, and the retention of T cells within granulomatous foci. CXCL, chemokine (C-X-C motif) ligand 1.

(1). Analyzing the expression of adhesion molecules with a PCR gene array demonstrated a significant up-regulation of integrin αX (ItgαX) (CD11c, a known dendritic cell marker, with an 11-fold increase at 60 days, and a 12-fold increase at 90 days), ItgαE (a threefold increase at 60 and 90 days), and Itgβ2 (a fivefold increase at 60 and 90 days) (Figure 5b).

DISCUSSION

The present study of MWCNT-induced lung granulomas provides a platform for mechanistic studies into granuloma biology. Other models produce a resolution of granulomas in 14–21 days, which may only represent the acute phase of granulomatous inflammation. Our studies demonstrated that: (*1*) MWCNTs cause persistent granulomatous inflammation for up to 90 days, (*2*) granulomas are composed of macrophages and $CD3^+$ T cells that are mostly $CD4^+$ cells, (*3*) osteopontin gene and protein expression are detected in alveolar macrophages and granulomatous foci, (*4*) distinct matrix metalloproteases are differentially expressed within granulomatous foci, and (*5*) granulomatous foci show a selective expression of cell adhesion molecules. The chronic nature of this model allows for the tracking of sequential events involved in the formation and persistence of granulomas.

Granulomatous inflammation is a phenomenon triggered by a wide variety of insults (e.g., parasitic, fungal, mycobacterial, or foreign body). However, regardless of etiology, common mechanisms are involved in the formation of granulomas. A series of complex, coordinated events brings about the recruitment of macrophages, T cells, cytokine release, and subsequent transformation of macrophages into epithelioid and multinucleated giant cells (17, 20, 29–32). Previous studies administered single and multiwall carbon nanotubes, and reported inflammatory lung responses (10, 12, 33). These studies yielded pathological lung lesions resembling granulomas. However, the recruited cellular populations and profiles of extracellular matrix gene expression within these lesions were not characterized. We demonstrated that after the administration of MWCNTs, large numbers of aggregates remained in the lungs of mice for up to 90 days, surrounded by macrophages and T cells. The present model of MWCNTs with chronic persistence of granulomas should alleviate the concerns raised by the data from earlier granuloma studies, which may only reflect events during the initial or resolution phases.

The administration of MWCNTs via oropharyngeal instillation as a bolus differs from real environmental exposure. Although this may be considered a limitation, the retropharyngeal instillation approach obtains a robust inflammatory response, expedites delivery, and achieves consistent lung exposure. Compared with other methods such as aerosol delivery, retropharyngeal instillation may be superior, because it achieves full and consistent delivery, with decreased variability between exposures (34, 35). A single comparative study of inhalation versus instillation demonstrated a smaller particle size and diminished lung inflammatory reaction with the inhalation instead of instillation of particles (33). However, investigations of the long-term effects from inhalations versus instillations demonstrated similar results for both techniques (36, 37). Although we observed a nascent response at 10 days, our intent was to analyze the chronic phase. Therefore, the analysis was focused on results at 60 and 90 days.

Osteopontin (OPN) expression is up-regulated in granulomas of multiple etiologies. Osteopontin is a chemotactic cytokine promoting adhesion and the modulating function of T cells, macrophages, and fibroblasts, and in its absence, the formation of granulomas is dampened (17, 38). Studies demonstrated an increase in metalloproteinases in the BAL of patients with granulomatous inflammation (18, 39). In the present study, MMP-12 increased in both BAL cells and granulomatous foci, with a concomitant and significant down-regulation of TIMP-3 at 60 and 90 days after exposure to MWCNTs. This finding suggests an environment where MMP-12 is unopposed by tissue inhibitors, allowing for the proteolytic cleavage of possibly OPN or other chemokines. MMP-12 is known to be induced by OPN (17), and we found an elevation of OPN in the BAL of all exposed mice. This would explain the observed elevation of MMP-12 in nongranulomatous tissue at 60 and 90 days. Future studies will be required to determine whether OPN biological effects are altered by the changes observed in the mRNA expression of MMP12 and TIMP-3 in lung tissues of MWCNT-exposed mice.

The formation of multinucleated giant cells, a key feature of granulomas, entails macrophage fusion through the binding of various cell-adhesion molecules (integrin types α and β) (1, 17,

18, 40, 41). The increased expression of integrins occurs in a variety of granulomatous disorders. Human studies associated the expression of Itgα_E with a fibrotic phenotype in patients with sarcoidosis (38). High concentrations of Itgβ2 (CD18) were reported in the sera of patients with sarcoidosis and in the peripheral blood monocytes of patients with *Mycobacterium tuberculosis* infection (42, 43). Itgβ2 is essential for cell–cell interactions between leukocytes during the formation of granulomas. In our model, an up-regulation of Itgα_X (CD11c), a marker for dendritic cells, was detected. Dendritic cells participate in granulomatous inflammation as antigen-presenting cells (44). Elevated Itgα_E (CD103) gene expression was also encountered, and this integrin is needed for the retention of intraepithelial lymphocytes in the mucosal tissues of the gut, urogenital tract, and lung (45, 46). Finally, in granulomatous foci, we found up-regulated Itgβ2 mRNA gene expression, which is believed to be necessary for cell–cell interactions between leukocytes during the formation of granulomas (42, 43).

Evidence from the present study and the literature is summarized in Figure 6, and suggests that an initial injury triggers the alveolar macrophage secretion of several cytokines, with a further recruitment of alveolar macrophages and T cells. Once on site, macrophages produce MMPs that alter cytokine signaling due to the proteolytic cleavage of osteopontin (18). The fragments resulting from the cleavage bind to integrins and lead to macrophage transformation and an increase in cell-adhesion molecules, promoting the formation of multinucleated giant cells and the retention of T cells. The sum of these events brings about the persistence of granulomatous inflammation.

The formation of granulomas is an initial response to injury. However, when this process continues unrestricted, disease ultimately ensues. Despite years of research, little progress has been achieved in controlling diseases resulting from unresolved granulomatous inflammation. Animal models previously used to investigate chronic lung granulomatous inflammation bear a pathological resemblance, but lack the chronicity observed in human granulomatous disease (9). Because of the rapid resolution of granulomas in these animal models, studies of the mechanisms responsible for the persistence of granulomas have been difficult. The use of retropharyngeal aspiration of MWCNTs to model lung granulomas represents a significant advance compared with the previously described models involving intravenous sepharose beads, and extends the persistence of granulomas from 14–21 days to more than 90 days. This MWCNT model of chronic granulomas contains many of the key characteristics that occur in human granulomatous disease (e.g., increased osteopontin, MMPs, and integrins). Because of the chronicity of this model and the potential for additional manipulations by combining this model with altered genetic backgrounds (null or transgenic models) and/or MWCNTs coupled to previously implicated antigens, our model presents a promising platform to explore essential components and promote a further understanding of the elusive biological mechanisms underlying the persistence of granulomas.

Author Disclosure: None of the authors has a financial relationship with a commercial entity that has an interest in the subject of this manuscript.

References

1. Helming L, Gordon S. The molecular basis of macrophage fusion. *Immunobiology* 2007;212:785–793.
2. Castranova V. Signaling pathways controlling the production of inflammatory mediators in response to crystalline silica exposure: role of reactive oxygen/nitrogen species. *Free Radic Biol Med* 2004;37: 916–925.
3. Baughman RP, Lower EE, du Bois RM. Sarcoidosis. *Lancet* 2003;361: 1111–1118.
4. Pagnoux C. Churg-Strauss syndrome: evolving concepts. *Discov Med* 2010;9:243–252.
5. Wieczorek S, Holle JU, Epplen JT. Recent progress in the genetics of Wegener's granulomatosis and Churg-Strauss syndrome. *Curr Opin Rheumatol* 2010;22:8–14.
6. Gauhar UA, Gaffo AL, Alarcon GS. Pulmonary manifestations of rheumatoid arthritis. *Semin Respir Crit Care Med* 2007;28:430–440.
7. Williams GT, Williams WJ. Granulomatous inflammation: a review. *J Clin Pathol* 1983;36:723–733.
8. Chensue SW, Otterness IG, Higashi GI, Forsch CS, Kunkel SL. Monokine production by hypersensitivity (*Schistosoma mansoni* egg) and foreign body (Sephadex bead)–type granuloma macrophages: evidence for sequential production of IL-1 and tumor necrosis factor. *J Immunol* 1989;142:1281–1286.
9. Kunkel S, Lukacs NW, Strieter RM, Chensue SW. Animal models of granulomatous inflammation. *Semin Respir Infect* 1998;13:221–228.
10. Lam CW, James JT, McCluskey R, Arepalli S, Hunter RL. A review of carbon nanotube toxicity and assessment of potential occupational and environmental health risks. *Crit Rev Toxicol* 2006;36:189–217.
11. Hirano S. A current overview of health effect research on nanoparticles. *Environ Health Prev Med* 2009;14:223–225.
12. Shvedova AA, Kisin ER, Porter D, Schulte P, Kagan VE, Fadeel B, Castranova V. Mechanisms of pulmonary toxicity and medical applications of carbon nanotubes: two faces of Janus? *Pharmacol Ther* 2009;121:192–204.
13. Izbicki G, Chavko R, Banauch GI, Weiden MD, Berger KI, Aldrich TK, Hall C, Kelly KJ, Prezant DJ. World Trade Center "sarcoid-like" granulomatous pulmonary disease in New York City Fire Department rescue workers. *Chest* 2007;131:1414–1423.
14. Kern DG, Neill MA, Wrenn DS, Varone JC. Investigation of a unique time–space cluster of sarcoidosis in Firefighters. *Am Rev Respir Dis* 1993;148:974–980.
15. Miller A. Sarcoidosis, firefighters' sarcoidosis, and World Trade Center "sarcoid-like" granulomatous pulmonary disease. *Chest* 2007;132:2053.
16. Prezant DJ, Dhala A, Goldstein A, Janus D, Ortiz F, Aldrich TK, Kelly KJ. The incidence, prevalence, and severity of sarcoidosis in New York City firefighters. *Chest* 1999;116:1183–1193.
17. O'Regan A. The role of osteopontin in lung disease. *Cytokine Growth Factor Rev* 2003;14:479–488.
18. Maeda K, Takahashi K, Takahashi F, Tamura N, Maeda M, Kon S, Uede T, Fukuchi Y. Distinct roles of osteopontin fragments in the development of the pulmonary involvement in sarcoidosis. *Lung* 2001;179:279–291.
19. Li X, O'Regan AW, Berman JS. IFN-g induction of osteopontin expression in human monocytoid cells. *J Interferon Cytokine Res* 2003;23:259–265.
20. Nishikaku AS, Scavone R, Molina RF, Albe BP, Cunha CS, Burger E. Osteopontin involvement in granuloma formation and in the severity of *Paracoccidioides brasiliensis* infection. *Med Mycol* 2009;47:495–507.
21. O'Regan AW, Hayden JM, Body S, Liaw L, Mulligan N, Goetschkes M, Berman JS. Abnormal pulmonary granuloma formation in osteopontin-deficient mice. *Am J Respir Crit Care Med* 2001;164:2243–2247.
22. Malur A, Mccoy AJ, Arce S, Barna BP, Kavuru MS, Malur AG, Thomassen MJ. Deletion of PPAR gamma in alveolar macrophages is associated with a Th-1 pulmonary inflammatory response. *J Immunol* 2009;182:5816–5822.
23. Livak KJ, Schmittgen TD. Analysis of relative gene expression data using real-time quantitative PCR and the 2(−delta delta C(T)) method. *Methods* 2001;25:402–408.
24. Brunauer S, Love KS, Keenan RG. Adsorption of nitrogen and the mechanism of ammonia decomposition over iron catalysts. *J Am Chem Soc* 1942;64:751–758.
25. Barrett EP, Joyner LG, Halenda PP. The determination of pore volume and area distributions in porous substances: I. Computations from nitrogen isotherms. *J Am Chem Soc* 1951;73:373–380.
26. Nishikaku AS, Molina RF, Ribeiro LC, Scavone R, Albe BP, Cunha CS, Burger E. Nitric oxide participation in granulomatous response induced by *Paracoccidioides brasiliensis* infection in mice. *Med Microbiol Immunol (Berl)* 2009;198:123–135.
27. Agostini C, Meneghin A, Semenzato G. T-lymphocytes and cytokines in sarcoidosis. *Curr Opin Pulm Med* 2002;8:435–440.
28. Co DO, Hogan LH, Il-Kim S, Sandor M. T cell contributions to the different phases of granuloma formation. *Immunol Lett* 2004;92:135–142.
29. Algood HM, Lin PL, Flynn JL. Tumor necrosis factor and chemokine interactions in the formation and maintenance of granulomas in tuberculosis. *Clin Infect Dis* 2005;41:S189–S193.

30. Chensue SW, Warmington K, Ruth JH, Lukacs N, Kunkel SL. Mycobacterial and schistosomal antigen-elicited granuloma formation in IFN-gamma and IL-4 knockout mice: analysis of local and regional cytokine and chemokine networks. *J Immunol* 1997;159: 3565–3573.
31. Saunders BM, Cooper AM. Restraining mycobacteria: role of granulomas in mycobacterial infections. *Immunol Cell Biol* 2000;78:334–341.
32. Wallis RS, Broder MS, Wong JY, Hanson ME, Beenhouwer DO. Granulomatous infectious diseases associated with tumor necrosis factor antagonists. *Clin Infect Dis* 2004;38:1261–1265.
33. Li JG, Li WX, Xu JY, Cai XQ, Liu RL, Li YJ, Zhao QF, Li QN. Comparative study of pathological lesions induced by multiwalled carbon nanotubes in lungs of mice by intratracheal instillation and inhalation. *Environ Toxicol* 2007;22:415–421.
34. Foster WM, Walters DM, Longphre M, Macri K, Miller LM. Methodology for the measurement of mucociliary function in the mouse by scintigraphy. *J Appl Physiol* 2001;90:1111–1117.
35. Su X, Looney M, Robriquet L, Fang X, Matthay MA. Direct visual instillation as a method for efficient delivery of fluid into the distal airspaces of anesthetized mice. *Exp Lung Res* 2004;30:479–493.
36. Costa DL, Lehmann JR, Winsett D, Richards J, Ledbetter AD, Dreher KL. Comparative pulmonary toxicological assessment of oil combustion particles following inhalation or instillation exposure. *Toxicol Sci* 2006;91:237–246.
37. Driscoll KE, Costa DL, Hatch G, Henderson R, Oberdorster G, Salem H, Schlesinger RB. Intratracheal instillation as an exposure technique for the evaluation of respiratory tract toxicity: uses and limitations. *Toxicol Sci* 2000;55:24–35.
38. Pardo A, Gibson K, Cisneros J, Richards TJ, Yang Y, Becerril C, Yousem S, Herrera I, Ruiz V, Selman M, *et al.* Up-regulation and profibrotic role of osteopontin in human idiopathic pulmonary fibrosis. *PLoS Med* 2005;2:e251.
39. Henry MT, McMahon K, Mackarel AJ, Prikk K, Sorsa T, Maisi P, Sepper R, Fitzgerald MX, O'Connor CM. Matrix metalloproteinases and tissue inhibitor of metalloproteinase–1 in sarcoidosis and IPF. *Eur Respir J* 2002;20:1220–1227.
40. MacLauchlan S, Skokos EA, Meznarich N, Zhu DH, Raoof S, Shipley JM, Senior RM, Bornstein P, Kyriakides TR. Macrophage fusion, giant cell formation, and the foreign body response require matrix metalloproteinase 9. *J Leukoc Biol* 2009;85:617–626.
41. Barry ST, Ludbrook SB, Murrison E, Horgan CM. Analysis of the alpha4beta1 integrin–osteopontin interaction. *Exp Cell Res* 2000;258: 342–351.
42. Hamblin AS, Shakoor Z, Kapahi P, Haskard D. Circulating adhesion molecules in sarcoidosis. *Clin Exp Immunol* 1994;96:335–338.
43. Yassin RJ, Hamblin AS. Altered expression of CD11/CD18 on the peripheral blood phagocytes of patients with tuberculosis. *Clin Exp Immunol* 1994;97:120–125.
44. Hume DA. Macrophages as APC and the dendritic cell myth. *J Immunol* 2008;181:5829–5835.
45. Cepek KL, Shaw SK, Parker CM, Russell GJ, Morrow JS, Rimm DL, Brenner MB. Adhesion between epithelial cells and T lymphocytes mediated by E-cadherin and the alpha E beta 7 integrin. *Nature* 1994;372:190–193.
46. Erle DJ, Brown T, Christian D, Aris R. Lung epithelial lining fluid T cell subsets defined by distinct patterns of beta 7 and beta 1 integrin expression. *Am J Respir Cell Mol Biol* 1994;10:237–244.